Faithful Effective-One-Body waveforms of equal-mass coalescing black-hole binaries

Thibault Damour,^{1,2} Alessandro Nagar*,^{1,2} Ernst Nils Dorband,³ Denis Pollney,³ and Luciano Rezzolla^{3,4}

¹ Institut des Hautes Etudes Scientifiques, 91440 Bures-sur-Yvette, France

¹Institut des Hautes Etudes Scientifiques, 91440 Bures-sur-Yvette, France

²ICRANet, 65122 Pescara, Italy

³Max-Planck-Institut für Gravitationsphysik, Albert-Einstein-Institut, Potsdam-Golm, Germany

⁴Department of Physics and Astronomy, Louisiana State University, Baton Rouge, LA, USA

(Dated: January 22, 2008)

We continue the program of constructing, within the Effective-One-Body (EOB) approach, high-accuracy analytic waveforms describing the signal emitted by inspiralling and coalescing black hole binaries. Here, we compare a recently derived, resummed 3 PN-accurate EOB quadrupolar waveform to the results of a numerical simulation of the inspiral and merger of an equal-mass black hole binary. We find a remarkable agreement, both in phase and in amplitude, with a maximal dephasing which can be reduced below ± 0.005 gravitational-wave (GW) cycles over 12 GW cycles corresponding to the end of the inspiral, the plunge, the merger and the beginning of the ringdown. This level of agreement is shown for two different values of the effective 4 PN parameter a_5 , and for corresponding, appropriately "flexed" values of the radiation-reaction resummation parameter $v_{\rm pole}$. In addition, our resummed EOB amplitude agrees to better than the 1% level with the numerical-relativity one up to the late inspiral. These results, together with other recent work on the EOB-numerical-relativity comparison, confirm the ability of the EOB formalism to faithfully capture the general relativistic waveforms.

PACS numbers: 04.25.Nx, 04.30.-w, 04.30.Db

I. INTRODUCTION

The gravitational-wave (GW) signals emitted by coalescing black hole binaries are among the most promising targets for the currently operating network of ground-based detectors GEO/LIGO/Virgo. The most useful part of the waveform for detection comes from the most relativistic part of the dynamics, around the coalescence, i.e. the last few cycles of the adiabatic inspiral, the plunge and the merger. In order to successfully detect GWs from coalescing black hole binaries and to be able to reliably measure the source physical parameters, one needs to have in advance a large bank of "templates" that accurately represent the GW waveforms emitted by these binaries. In the terminology of [1] one needs templates that are both effectual and faithful¹. The construction of faithful GW templates for coalescing binaries comprising spinning black holes (with arbitrary masses m_1 , m_2 and spins S_1 , S_2) poses a difficult challenge. Due to the multi-dimensionality of the corresponding parameter space, state-of-the-art numerical simulations cannot densely sample this parameter space. This motivates the need to develop analytical methods for computing (as a function of the physical parameters m_1 , m_2 , S_1 , S_2) the corresponding waveforms. The Effective-One-Body (EOB) method [2–5] was developed to analytically represent the motion of, and radiation from, coalescing binary black holes with arbitrary masses and spins. This method was the

first to provide estimates of the complete waveform (covering inspiral, plunge, merger and ring-down) of a coalescing black hole binary, both for non-spinning systems [3], and for spinning ones [6].

Numerical Relativity (NR) recently succeeded in giving us access to reliable information about the dynamics and radiation of binary black hole coalescences [7–18]. This opens the possibility of comparing the EOB predictions to NR results.

The comparison between the EOB approach and NR results has been recently initiated in several works [19-24]. These recent comparisons have been done using two different versions of EOB waveforms. The works of Buonanno et al. [19, 20, 23] used a restricted waveform, as proposed in the pioneering EOB paper [3] (but with an improved matching to the ringdown making use of three quasi-normal modes). By contrast, the recent works of Damour and Nagar [22, 24] use a new, resummed 3 PN-accurate EOB quadrupolar waveform. This improved EOB waveform has been shown to exhibit a remarkable agreement, both in phase and in amplitude, with NR waveforms in two separate physical situations: (i) inspiral and coalescence of small-mass-ratio (non-spinning) systems [22] (comparing it to waveforms computed by means of numerical simulations of test particles, with an added radiation-reaction force, moving in black-hole backgrounds [25]) and (ii) inspiral (up to a limiting GW frequency $\sim 0.14/M$) of an equalmass (non-spinning) system [24] (comparing it to recently published results of a high-accuracy inspiral simulation [18]). In other words, the improved EOB waveform has been able, in these two cases, to provide faithful GW templates.

The present paper is a continuation of the general program of constructing, within the Effective-One-Body (EOB) approach, high accuracy, faithful analytic waveforms describing the gravitational wave signal emitted by inspiralling and coalescing binary black holes. Here we shall consider the *coalescence signal* emitted by a non-spinning *equal-mass* binary

^{*}Supported by a fellowship from the Istituto Nazionale di Fisica Nucleare (Italy).

¹ In brief, "effectual templates" are templates exhibiting large overlaps with an exact signal after maximizing over all (kinematical and dynamical) parameters, while "faithful" ones are so "close" to an exact one that they have large overlaps for values of the dynamical parameters which are very close to the real ones ("small biases").

black-hole system. We shall compare the phase and the amplitude of the new *resummed* 3 PN-accurate EOB quadrupolar waveform of [22, 24] to a numerical relativity simulation of a coalescing black hole binary performed at the Albert Einstein Institute (AEI).

This comparison will confirm the ability of the EOB approach in providing accurate analytical representations of NR waveforms. We note that the recent work [23] had already shown the ability of the less accurate restricted EOB waveforms to provide effectual coalescence waveforms for several different mass ratios $(m_1/m_2 = 1, 3/2, 2 \text{ and } 4)$, and to provide, for instance, near-faithful waveforms in the equal mass case, in the sense of having a dephasing, with respect to NASA-Goddard NR waveforms, of $\sim \pm 0.03$ GW cycles over 15 GW cycles. The present paper will show that the new, resummed waveform exhibits an even smaller dephasing $\sim \pm 0.005$ GW cycles over 12 GW cycles, and, most remarkably, exhibits an excellent agreement in amplitude, both during the inspiral and the ring-down. This good result is obtained by making use (as proposed in several previous works [5, 23, 24, 26, 27]) of the natural flexibility of the EOB approach.

Let us also mention, as alternative approach to the construction of analytical template waveforms to model the inspiral, merger and ringdown stages of the coalescence of nonspinning binary black holes with arbitrary mass ratios, the work of Refs. [28, 29].

This paper is organized as follows: In Sec. II we briefly describe the numerical simulation, whose results we use in the following. In Sec. III we spell out the features of the EOB waveform that we shall use. The main section is Sec. IV where we compare the new, resummed EOB waveform to NR data. We also include a comparison where we use the kind of less accurate "restricted" EOB waveform, and simpler QNM-matching used in some of the previous EOB works [3, 19, 20, 23]. The paper ends by some conclusions.

II. BRIEF DESCRIPTION OF THE NUMERICAL SIMULATION

The numerical simulations have been carried out with the Ccatie code [30], a three-dimensional finite-differencing code developed at the Albert Einstein Institute and at the Center for Computation and Technology (CCT) of the Louisiana State University. The code is based on the Cactus Computational Toolkit [31] for the solution of the Einstein equations in a finite-size domain covered with a Cartesian rectangular grid. The main and new features of the code have been recently discussed in Ref. [30], and we here briefly recall the most important ones only.

The Einstein equations are formulated as an initial-value problem via a conformal and traceless "3+1" decomposition in which the spacetime is decomposed into three-dimensional spacelike slices, described by a 3-metric, its embedding in the full spacetime, specified by the extrinsic curvature, and the gauge functions: the lapse and the shift (see [30] for the explicit form of the equations). These gauge functions are

evolved using the "1+log" slicing condition for the lapse [32], while the shift is evolved using the hyperbolic $\tilde{\Gamma}$ -driver condition discussed in Ref. [33], but with the difference that advection terms have been added following the experience of [8, 34], and are required for correct advection of the punctures in "moving-puncture" evolutions.

Spatial differentiation of the evolution variables is performed via straightforward finite-differencing using fourth-order accurate centered stencils for all but the advection terms for each variable, which are instead upwinded in the direction of the shift. Vertex-centered adaptive mesh-refinement is employed using nested grids via the Carpet infrastructure [35], with a 2:1 refinement for successive grid levels, and the highest resolution concentrated in the neighborhood of the individual horizons. Individual apparent horizons are located every few time steps during the time evolution [36], which is obtained via a "method-of-lines" and with a fourth-order accurate Runge-Kutta time integrator.

The simulations were performed on a domain with outer boundaries located at $768M_c^2$, and a grid structure consists of nine mesh-refinement levels, the finest of which has a spatial resolution of $h = 0.02M_c$. Simulations with lower resolution (i.e., with $h = 0.024M_c$ and $h = 0.03M_c$) have also been carried out to validate the consistency of the results. An important feature of the Ccatie code is the possibility of employing two distinct methods for the calculation of the gravitational radiation produced. The first method uses the Newman-Penrose curvature scalar ψ_4 , with respect to a suitable frame at the extraction radius. An alternative method measures the metric of the numerically generated spacetime against a fixed background at the extraction radius, and determines the gauge-invariant Regge-Wheeler-Zerilli-Moncrief functions (see Ref. [37] for a review and references). Both methods have been systematically studied in Ref. [30], where they were also compared and shown to yield essentially identical results, both in terms of their asymptotic scaling properties (e.g., the peeling-theorem), and in terms of the polarization amplitudes h_+ and h_{\times} . The analysis carried out here used as basic NR data the gauge-invariant (Zerilli-Moncrief) metric perturbations. These were extracted on (NR) coordinate 2-spheres with (NR) coordinate radii $R_{\rm NR}=60M_c$ up to $R_{\rm NR}=120M_c$, with a separation of $10M_c$ between two adjacent observers. The analysis carried out below uses, as approximate asymptotic amplitude, the metric perturbation extracted at $R_{\rm NR} = 120 M_c$.

The initial data for the black-hole binary are obtained by a Brill-Lindquist [38] construction, where the additional asymptotically flat end of each wormhole is compactified into a single point, the so called *puncture* [39]. This approach explicitly uses the Bowen-York extrinsic curvature and solves the Hamiltonian constraint equation numerically as detailed in Ref. [40], and after the free parameters for the puncture initial

 $^{^2}$ We denote by M_c the internal length and mass units used in the code (with G=c=1). Beware that M_c slightly differs from $M=m_1+m_2$ (see below).

TABLE I: Initial ADM mass (scaled by $M=m_1+m_2$) and angular momentum of the spacetime (scaled by M^2); final mass (scaled by M) and dimensionless spin parameter $j_{\rm f}=J_{\rm f}/M_{\rm f}^2$ of the merged black hole; dominant (quasi-normal-mode) complex frequency of the ringdown; for two different grid spacings h.

h/M	$M_{ m ADM}/M$	$J_{\rm ADM}/M^2$	$M_{ m f}^{ m hor}/M$	$j_{ m f}^{ m hor}$	$M_{ m f}^{ m ring}/M$	$j_{ m f}^{ m ring}$	$M\sigma_{2220}^{+}$
0.024	0.990484	0.991803	0.951531	0.687142	_	_	
0.020	0.990484	0.991803	0.951611	0.686916	0.959165	0.684639	$0.085475 + i\ 0.551040$

data are chosen. Quasi-circularity of the initial orbit can then be obtained by specifying the puncture parameters in terms of an effective-potential method [41] as discussed in [30]. However, the assumption of "quasi-circularity" (in the sense of [41]) at the (rather small) initial separations frequently used in numerical-relativity simulations has the drawback of introducing a small but nonzero amount of eccentricity. To compensate for, or reduce, this effect, other approaches have been suggested recently. One of these is based on an iterative minimization procedure where, throughout a series of simulations with slightly different initial black hole configurations, the eccentricity is measured and minimized [42]. A simpler and rather effective approach has been proposed in Ref. [43], and consists of specifying the initial puncture-parameters as the end-state of a binary system whose evolution is determined, starting from a large separation, via the solution of the Taylorexpanded 3 PN-accurate equations of motion [6, 44, 45].

We have here essentially followed this latter prescription and considered, in particular, the initial data denoted by E11 in Table I of [43], that have been shown there to reduce the eccentricity to e < 0.002. More specifically, our initial black holes have a coordinate distance $D = 11 M_c$, momenta in the radial and tangential directions of $P_r = -7.09412 \times 10^{-4} M_c$ and $P_t = 0.0900993 M_c$, and a puncture mass-parameter of $0.487035 M_c$, leading to initial individual black-hole masses $m_1 = m_2 = 0.499821 M_c$, and thus a total mass of the binary system $M = m_1 + m_2 = 0.999642 M_c$. Overall, the simulation covers about $\sim 1600 \, M$ of the final evolution of the binary, thus comprising 8 orbits and about 16 GW cycles.

The mass and spin of the final black hole have been computed through two different methods yielding, however, very similar results: (a) by using the isolated/dynamical horizon formalism [46, 47], where a proper rotational Killing vector is searched on the final apparent horizon to measure the spin, and the horizon area is used for computing the black hole mass (see Section IV D of Ref. [30] for details); (b) by performing a fit of the dominant quasi-normal mode³ of the *complex* ringdown waveform.

This fit was performed by a non-linear least-squares Gauss-Newton method, using $\exp(-\sigma t + \rho)$ as parameter–dependent template (with two *complex* parameters (σ, ρ)), and an appropriate time interval during the ringdown (chosen by minimiz-

ing the post-fit residual). [For discussion of methods for QNM fitting see Refs. [48–50]]. Then, from the best-fit value of σ (i.e., the QNM dominant complex frequency σ_{2220}^+), we computed the values of the mass and dimensionless spin parameters of the final black hole by using the interpolating fits given in Appendix E of Ref. [51]. The results of these two methods are denoted as $(M^{\rm hor},j^{\rm hor})$ and $(M^{\rm ring},j^{\rm ring})$, respectively.

The most relevant properties of the binary system are summarized in Table I. The difference (which is $\lesssim 1\%$) between the quoted values of the final black hole parameters might come, in part, from inaccuracies in the interpolating fits of Ref. [51]. In the following we will use, in our EOB-matching procedure, the ringdown–fitted black hole parameters $(M^{\rm ring},j^{\rm ring})$ (so that the dominant complex frequency will be guaranteed to have the best possible value).

III. EFFECTIVE-ONE-BODY (EOB) METHOD AND WAVEFORM

We shall not review here in detail the EOB method [2–5], which has been described in several recent publications, notably Refs. [23, 24]. We shall only indicate the EOB elements that are crucial for the present study. For detailed definitions of the EOB ingredients we refer to the recent paper [24] that we follow, except when otherwise indicated below.

Before entering the details of our EOB implementation, let us recall that Ref. [24] proposed a methodology for improving the waveform implementation of the EOB philosophy based on understanding, element by element, the physics behind each feature of the waveform, and on systematically comparing various EOB-based waveforms with "exact" waveforms obtained by numerical relativity approaches. The first step of the methodology consisted in studying the small-mass-ratio limit, $\nu \equiv m_1 m_2/M^2 \ll 1$, in which one can use the well controllable "laboratory" of numerical simulations of test particles (with an added radiation-reaction force) moving in black hole backgrounds. Historically, this "laboratory" has been important in understanding/discovering several key features of GW emission near black holes. A notable example of this being the work of Davis, Ruffini and Tiomno [52] which discovered the transition between the plunge signal and a ringing tail when a particle falls into a black hole. The recent study of inspiralling and merging small-mass-ratio systems [22] led to introducing (and testing) the following improvements in EOB dynamics and waveforms: (i) an improved analytical expression for the $((\ell, m) = (2, 2))$ even-parity Zerilli-

³ In the notation introduced in Sec. III below, the dominant mode corresponds to the labels $(\pm, \ell, \ell', m, n) = (+, 2, 2, 2, 0)$.

Moncrief) waveform $\Psi_{22}^{(e)}$ which includes a resummation of the tail effects, and a 3 PN-accurate "non-linear" amplitude correction, (ii) the inclusion of non-quasi-circular corrections to the waveform, (iii) the inclusion of non-quasi-circular corrections to radiation reaction, and (iv) an improved treatment of the matching between the plunge and ring-down waveforms which takes into account a new understanding of the importance of the number of quasi-normal-modes (QNMs), the sign of their frequencies, and the length of the interval on which the matching is done. The resulting improved implementation (when $\nu \ll 1$) of the EOB approach yielded very faithful waveforms whose amplitude and phase agreed remarkably well with the "exact" ones: in particular, the EOB phasing differed from the "exact" one by less than $\pm 1.1\%$ of a cycle over the whole process.

The program initiated in [22] was pursued in [24] where the comparable-mass version of the improved, resummed 3^{+2} -PN accurate waveform was compared with the recently published inspiral simulation of the Caltech-Cornell group [18]. It was found that, by exploiting the combined flexibility in a_5 and $v_{\rm pole}$, one could reach a remarkable phase agreement, better than $0.001~{\rm GW}$ cycles over 30 GW cycles. Here, we shall similarly exploit the flexibility in a_5 and $v_{\rm pole}$ to best fit the AEI merger waveform.

Let us recall that the EOB approach is a *non-perturbatively resummed* analytic technique which consists of several different elements:

- an *Hamiltonian H*_{real} describing the conservative part of the relative two-body dynamics. The key ingredient of this Hamiltonian (defined in Eqs. (13) and (14) of [24]) is the "radial potential" A(r).⁵. This radial potential is defined, at n-Post-Newtonian (PN) order, as the (1,n) Padé resummation [4] of its Taylor (i.e. usual PN) expansion (written in Eq. (15) of [24]).
- a radiation reaction force \mathcal{F}_{φ} (denoted $\hat{\mathcal{F}}_{\varphi}$ after its rescaling by $1/\mu$), which is defined as a Padé resummation [1] of its Taylor expansion (see Eq. (17) of [24]).
- an *improved "post-post-adiabatic"* dynamical initial data (positions and momenta) as advocated in Sec. III B of [24]. This procedure leads to negligible eccentricity when starting the integration of the EOB equations of motion at radius r=15.
- an improved, resummed "inspiral-plus-plunge" (here-

after abbreviated as "insplunge") waveform⁶ of the form

$$\left(\frac{c^2}{GM}\right)\Psi_{22}^{\text{insplunge}}(t) = -4\sqrt{\frac{\pi}{30}}\nu(r_{\omega}\Omega)^2 f_{22}^{\text{NQC}} F_{22} e^{-2i\Phi} ,$$
(1)

where $\Phi(t)$ is the EOB orbital phase, $\Omega=\dot{\Phi}$ is the EOB orbital frequency, $r_{\omega}\equiv\psi^{1/3}$ is a modified EOB radius, with ψ being defined in Eq. (22) of Ref. [53]. The factor F_{22} is a resummed, 3^{+2} -PN-accurate complex amplitude correction valid during the (adiabatic) inspiral, and $f_{22}^{\rm NQC}$ is an extra complex correcting factor, aimed at taking care (in an effective way) of various non quasicircular (NQC) effects during the plunge. F_{22} is defined in Eqs. (5)-(11) of [24], with f_{22} being the (3,2) Padé resummation of $f_{22}^{\rm Taylor}$.

• a ringdown waveform

$$\Psi_{22}^{\text{ringdown}}(t) = \sum_{N} C_{N}^{+} e^{-\sigma_{N}^{+} t} + \sum_{N} C_{N}^{-} e^{-\sigma_{N}^{-} t} , \quad (2)$$

where the label N actually refers to a set of indices (ℓ,ℓ',m,n) , with $(\ell,m)=(2,2)$ being the Schwarzschild-background multipolarity degrees of the considered (Zerilli-Moncrief-type) waveform $\Psi_{\ell m} \sim h_{\ell m}$, with $n=0,1,2,\ldots$ being the "overtone number" of the considered Kerr-background Quasi-Normal Mode (QNM; n=0 denoting the fundamental mode), and ℓ' the degree of its associated spheroidal harmonics $S_{\ell'm}(a\sigma,\theta)$. In addition $\sigma_N^{\pm}=\alpha_N^{\pm}\pm \mathrm{i}\omega_N^{\pm}$ refers to the positive/negative complex QNM frequencies $(\alpha_N^{\pm}>0)$ and $(\alpha_N^{\pm}>0)$ indicate the inverse damping time and the oscillation frequency of each mode respectively). The sum over $(\alpha_N^{\pm}>0)$ (used as expansion basis to define $(\alpha_N^{\pm}>0)$) (used as expansion basis to define $(\alpha_N^{\pm}>0)$) (used an e

• an improved way of *matching* the inspiral-plus-plunge waveform to the ring-down one, on a multi-toothed "comb" $(t_m - p\delta, t_m - (p-1)\delta, \ldots, t_m - \delta, t_m, t_m + \delta, \ldots, t_m + p\delta)$, centered around some "matching" time t_m .

⁴ The notation 3^{+2} -PN refers here to the fact that F_{22} resums not only the known ν -dependent 3 PN waveform corrections, but also the $\nu=0$ limit of the 4 PN and 5 PN waveform amplitude corrections. See [24] for details and references.

⁵ Except when said otherwise, we henceforth systematically scale dimensionful quantities by means of the total rest mass $M \equiv m_1 + m_2$ of the binary system. For instance, we use the dimensionless EOB radial coordinate $r \equiv R_{\rm EOB}/M$, with G = 1. Note also that $\nu \equiv \mu/M$ with $\mu \equiv m_1 m_2/M$.

⁶ Here, as before, we work with a *metric-level* ("h"), rather than curvature-level (" ψ_4 "), waveform. However, we normalize here this metric waveform in the same "Zerilli-Moncrief" way as in the test-mass work [22]. This differs simply by a numerical factor from both the usual tensor-spherical harmonics (ℓ,m) metric amplitude $h_{\ell m}$ and the related metric variables $Q_{\ell m}^{+,\times}$ extracted from the NR evolution [30]: $Rh_{\ell m} = \sqrt{(\ell+2)(\ell+1)\ell(\ell-1)} \left(\Psi_{\ell m}^{(e)} + \mathrm{i}\Psi_{\ell m}^{(o)}\right) = \frac{1}{\sqrt{2}} \left(Q_{\ell m}^{+} - \mathrm{i}\int_{-\infty}^{t} Q_{\ell m}^{\times}(t')dt'\right)$

• Finally, we define our complete EOB matched waveform (from $t=-\infty$ to $t=+\infty$) as

$$\Psi_{22}^{\text{EOB}}(t) \equiv \theta(t_m - t) \Psi_{22}^{\text{insplunge}}(t) + \theta(t - t_m) \Psi_{22}^{\text{ringdown}}(t)$$
 (3)

where $\theta(t)$ denotes Heaviside's step function. Note that, if one wanted to have a C^{∞} transition between the two waveforms one could replace $\theta(t-t_m)$ by one of Laurent Schwartz's well-known smoothed step functions (or "partitions of unity") $\theta_{\epsilon}((t-t_m)/(2p\delta))$.

Let us now state the specific choices made here for the various EOB ingredients just recalled. Some of these choices correspond to various ways of "flexing" the EOB formalism (in the sense of Ref. [26]).

- We "flex" the currently known 3 PN-accurate EOB Hamiltonian [4, 44] by introducing an (effective) 4 PN Hamiltonian parameter a_5 , parametrizing an additional contribution $+a_5\nu/r^5$ in the main EOB radial function A(r). This parameter has already been introduced (under varying notations) in several previous works [5, 23, 24, 26, 27].
- Similarly, the EOB radiation reaction force (defined by Eq. (17) of [24]) is "flexed" by allowing the Padéresummation parameter $v_{\rm pole}$ to differ from the "standard" value $v_{\rm pole}^{\rm DIS}(\nu)$ advocated in [1].

In addition, we shall also briefly explore another physically natural flexibility in the radiation reaction, which was introduced (and shown to be physically needed for faithfulness) in [22]: the multiplication of the radiation reaction by a non quasi-circular (NQC) correction factor $f_{\rm RR}^{\rm NQC}$.

- To define precisely the "insplunge waveform" (1) we need to specify:
 - (i) the argument x(t) used in the f_{22} "brick" within F_{22} (see Eq.(10) of [24]). We shall use here $x=\Omega^{2/3}$ where Ω is the *EOB orbital frequency*.
 - (ii) the Padé resummation of the Taylor expansion $f_{22}^{\rm Taylor}$ of f_{22} . As in [24] we shall use a P_2^3 Padé.
 - (iii) the definition of the non quasi-circular (NQC) correction factor $f_{22}^{\rm NQC}$. To do this we follow the rationale explained in [22]. For convenience, we choose (as suggested in footnote 9 of [22]) a *factorized* complex NQC factor

$$f_{22}^{\text{NQC}} = \left[1 + a \frac{p_{r_*}^2}{(r\Omega)^2 + \epsilon}\right] \exp\left(+ib \frac{p_{r_*}}{r\Omega}\right),$$
 (4)

in which a (denoted a' in the cited footnote) affects only the modulus, and b (alias b') only the phase. To ease some technical problems during the ring-down linked

to the fact that $\Omega(t)$ tends exponentially towards zero as $t \to +\infty$ we have added a ("cut-off") constant ϵ to the first denominator $(r\Omega)^2$. As discussed in [22], one can a priori analytically determine a "good" value of the NQC-modulus parameter a by requiring that the modulus of the full EOB insplunge waveform (1) be maximum at the "EOB-light-ring", i.e. when the EOB orbital frequency Ω reaches a maximum. Ref. [22] mentioned that, in the $\nu \ll 1$ limit, this requirement implied a = 1/2. We found, by numerically exploring the modulus of $\Psi_{22}^{\text{insplunge}}(t)$, that the same value, a=1/2 (together with $\epsilon = 0.12$), can be used in the case $\nu = 1/4$ considered here. Concerning the NQC-phase parameter b we simply choose b = 0. [Note that the comparablemass resummed EOB waveform of [24] uses a refined estimate for the additional phase δ_{22} of $\Psi_{22}^{\mathrm{insplunge}}(t)$ compared to the one used in [22].]

• Concerning the choice of QNMs we recall that the discussion of the physical excitation of QNMs in [22] (see the summary in Fig. 4 there) suggested that it is sufficient to use only *positive-frequency* QNMs in the ringdown waveform (2). This is what we shall do here as well.

A new feature of the comparable-mass case (w.r.t. the small ν limit) is the "mixing" between various ℓ' QNMs (with $\ell' \neq \ell$) that can enter a given (ℓ,m) multipolar wave. This mixing is due to the " $a\omega$ coupling" terms in the separated Teukolsky equations and has been discussed in [19, 54]. However, as emphasized in [19], this coupling has only a small effect on the $(\ell,m)=(2,2)$ waveform. We shall neglect it and consider only the (positive-frequency) QNM modes having the same values of (ℓ,m) as the considered multipolar waveform $h_{\ell m}$ (i.e. (2,2) in the present paper).

On the other hand, contrary to other recent implementations of the EOB approach [19, 20, 23], we shall use a matching comb with five teeth (p=2) and five (positive-frequency) QNMs $\sigma_{\ell mn}^+ = \alpha_{\ell mn}^+ + \mathrm{i}\omega_{\ell mn}^+$, with $\ell=2, m=+2$, and n=0,1,2,3,4. To estimate the values (as functions of the mass and spin of the final black hole) of the damping time and the oscillation frequency of each mode we did the following: (i) for the first three modes we used the approximate fitting formulas given in Appendix E of Ref. [51]; while, (ii) for the fourth and fifth modes (i.e. n = 3, 4) we noticed that the graphic results of [55] (notably his most relevant Fig. 4) exhibit an approximate linearity of the complex QNM frequency $\sigma_{\ell mn}^{\pm}$ as a function of the overtone number n. [Indeed, the corresponding points in the complex σ plane are approximately aligned.] We then exploited this approximate linearity to express the needed n=3and n = 4 complex frequencies as linear combinations of the above-discussed n = 1 and n = 2 ones.

 Concerning the *matching*, on a multi-toothed "comb", of the inspiral-plus-plunge waveform to the ring-down one we need to specify the two parameters defining such a comb, namely the central "matching" time t_m , and the spacing between the teeth of the comb: $\delta = \Delta t/4^7$. In conformity with the basic idea proposed in the original EOB paper [3] we choose as central matching time t_m the so-called "EOB light-ring crossing" time; i.e., the EOB dynamical time when the EOB orbital frequency Ω reaches its maximum. See [22] for a detailed discussion of why such a choice is physically preferred. Concerning the choice of the comb spacing δ , we expect from [22] that a value of order $\delta = (7.2M)/4 = 1.8M$ will be good. Below, we shall explore values near this one.

IV. COMPARING THE NR WAVEFORM TO EOB ONES

As explained in Sec. II, the basic NR data that we shall consider is a time-series giving the quadrupolar $[(\ell, m) = (2, 2), \text{Zerilli-Moncrief-normalized}]$ metric waveform Ψ_{22}^{NR} as a function of the NR time variable t_{NR} (measured in units of $M \equiv m_1 + m_2$). $\Psi_{22}^{\text{NR}}(t_{\text{NR}})$ is a complex number. The NR results consist of the real and imaginary parts of Ψ_{22}^{NR} . It is, however, more convenient to decompose the complex waveform in modulus (or amplitude) and phase, say

$$\Psi_{22}^{\text{NR}}(t_{\text{NR}}) = A_{22}^{\text{NR}}(t_{\text{NR}}) \exp\left(-\mathrm{i}\phi_{22}^{\text{NR}}(t_{\text{NR}})\right).$$
 (5)

The 2π ambiguity in the phase is fixed by starting with the principal value of the argument of Ψ^{NR}_{22} at the beginning of the NR simulation, and then keeping track of the 2π turns as the waveform continuously unfolds.

One can then compute the gravitational wave (GW) frequency as a function of time by (numerically) differentiating the GW phase

$$\omega_{22}^{\rm NR}(t_{\rm NR}) = \frac{d\phi_{22}^{\rm NR}}{dt_{\rm NR}}.\tag{6}$$

[It can equivalently be obtained by computing the imaginary part of the logarithmic time derivative of $\Psi_{22}^{\rm NR}(t_{\rm NR})$.]

As emphasized in [24], another useful diagnostics of GW radiation is the GW phase acceleration $\alpha=d\omega/dt=d^2\phi/dt^2$ considered as a function of the GW frequency ω . However, because of the presence of some additional high-frequency wiggles in ϕ and ω in the NR data, we shall not consider here the phase-acceleration curve $\alpha(\omega)$. Instead, we shall directly compare the numerical GW amplitude, phase and frequency to their analytical, EOB counterparts.

The integration of the basic EOB dynamical equations (written in [24]) gives, for each chosen value of the EOB "flexibility parameters" (notably a_5 and $v_{\rm Pole}$), several important time series, and notably: (i) the EOB orbital frequency $\Omega(t_{\rm EOB})$, where $t_{\rm EOB}$ is the EOB dynamical time scale (measured in units of M); (ii) the new, resummed matched 3^{+2} -PN-accurate quadrupolar EOB waveform $\Psi^{\rm EOB}_{22}(t_{\rm EOB})$; then, from the latter, one can define (as for the NR case) the corresponding EOB amplitude, $A^{\rm EOB}_{22}(t_{\rm EOB})$, EOB phase, $\phi^{\rm EOB}_{22}(t_{\rm EOB})$, and EOB frequency $\omega^{\rm EOB}_{22}(t_{\rm EOB})$. To compare the NR and EOB phase time-series $\phi^{\rm NR}_{22}(t_{\rm NR})$ and $\phi^{\rm EOB}_{22}(t_{\rm EOB})$ one needs to shift, by additive constants, both one of the time variables, and one of the phases. In other words, we need to determine τ and α such that the "shifted" EOB quantities

$$t'_{\rm EOB} = t_{\rm EOB} + \tau$$
, $\phi'^{\rm EOB}_{22} = \phi^{\rm EOB}_{22} + \alpha$ (7)

"best fit" the NR ones. One convenient way to do so is first to "pinch" the EOB/NR phase difference at two different instants (corresponding to two different frequencies). More precisely, one can choose two NR times $t_1^{\rm NR}, t_2^{\rm NR}$, which determine two corresponding GW frequencies $\omega_1 = \omega_{22}^{\rm NR}(t_1^{\rm NR})$, $\omega_2 = \omega_{22}^{\rm NR}(t_2^{\rm NR})$, and then find the time shift $\tau(\omega_1,\omega_2)$ such that the shifted EOB phase difference, between ω_1 and ω_2 , $\Delta\phi^{\rm EOB}(\tau) \equiv \phi_{22}^{\rm EOB}(t_2^{\rm EOB}) - \phi_{22}^{\rm EOB}(t_1^{\rm EOB}) = \phi_{22}^{\rm EOB}(t_2^{\rm EOB} + \tau) - \phi_{22}^{\rm EOB}(t_1^{\rm EOB} + \tau)$ is equal to the corresponding (unshifted) NR phase difference $\Delta\phi^{\rm NR} \equiv \phi_{22}^{\rm NR}(t_2^{\rm NR}) - \phi_{22}^{\rm NR}(t_1^{\rm NR})$. This yields one equation for one unknown (τ) , and (uniquely) determines a value $\tau(\omega_1,\omega_2)$ of τ . [Note that the $\omega_2 \to \omega_1 = \omega_m$ limit of this procedure yields the one-frequency matching procedure used in [18].] After having so determined τ , one can uniquely define a corresponding best-fit phase shift $\alpha(\omega_1,\omega_2)$ by requiring that, say, $\phi_{22}^{\rm EOB}(t_1^{\prime EOB}) \equiv \phi_{22}^{\rm EOB}(t_1^{\prime EOB}) + \alpha = \phi_{22}^{\rm NR}(t_1^{\rm NR})$.

Having so related the EOB time and phase variables to the NR ones we can straigthforwardly compare all the EOB time series to their NR correspondants. In particular, we can compute the (shifted) EOB–NR phase difference

$$\Delta^{\omega_1,\omega_2}\phi_{22}^{\text{EOBNR}}(t_{\text{NR}}) \equiv \phi_{22}^{'\text{EOB}}(t'^{\text{EOB}}) - \phi_{22}^{\text{NR}}(t^{\text{NR}}).$$
 (8)

In the following we will chose two matching instants (and corresponding frequencies) that take place during late inspiral and plunge, namely: $t_1^{\rm NR}=999.72,\,t_2^{\rm NR}=1494.94$ corresponding to $\omega_1=0.06815,\,\omega_2=0.2457$ (all expressed in M units).

To numerically implement the EOB/NR comparison we need to choose some values for the various "flexibility parameters" of the EOB framework. We have summarized above what are these parameters, and we have already indicated the values we chose for some of them. Among the remaining ones that need to be chosen, the two most crucial ones are a_5 and

 $^{^7}$ Note that in [22] we used the letter δ to denote the full width Δt of the comb

 $^{^8}$ As mentioned in Sec. II, we use the waveform extracted at a (coordinate) radius $R_{\rm NR}=120M_c\simeq 120M$, and $t_{\rm NR}$ is the time of the "observer" located at the latter radius.

 $^{^9}$ Alternatively, one can start by giving oneself ω_1,ω_2 and determine the NR instants $t_1^{\rm NR},t_2^{\rm NR}$ at which they are reached.

 $v_{\rm pole}$. Recently, Damour and Nagar have shown, by using some of the data published in [18], that the inspiral waveform (for GW frequencies smaller than about 0.14/M) could be remarkably well matched by the EOB one if one chose values of a_5 and v_{pole} following the rather precise correlation plotted in the upper panel of Fig. 3 in [24]. Here, as we are exploring a different physical regime (late inspiral, plunge and coalescence, with GW frequencies mostly larger than about 0.1/M), and comparing to a different set of numerical data. we shall not a priori impose the precise correlation between a_5 and v_{pole} found in [24]. However, we shall make use of some previous results suggesting a preferred range for the values of a_5 . On the one hand, Ref. [23] showed that the effectualness of (restricted) EOB waveforms against NR coalescence waveforms was largest when a_5 belonged to some rather wide interval (which also depended on the considered mass ratio). See Fig. 2 (right panel) in [23] from which one might conclude that a_5 lies probably between ~ 10 and ~ 100 . Buonanno et al. then chose $a_5 = 60$ as "best fit" value. On the other hand, Ref. [24] found that the phase agreement between (resummed) EOB waveforms and a rather long inspiral NR waveform was at its best when a_5 lied in a similarly wide interval (between ~ 10 and ~ 80) centered around $a_5 \sim 40$. In view of these results we shall focus, in the following, on two representative values of a_5 , namely $a_5 = 25$ (representative of the leftwardside of preferred a_5 values), and $a_5 = 60$ (representative of the rightward-side of preferred a_5 values, and chosen as best value by [23]). We have also checked that the values of a_5 between 25 and 60 lead (with appropriate choice of $v_{\rm pole}$) to results that are at least as good as the ones we shall exhibit below.

A. Comparing NR to resummed EOB for $a_5 = 25$

At this stage we have essentially fixed all the flexibility of the EOB formalism apart from the choices of $v_{\rm pole}$, and of the comb spacing δ . Among these two parameters, only the former one, $v_{\rm pole}$, is important for getting a very accurate phase agreement between EOB and NR. When $a_5=25$, we found (by trial and error) that 10 $v_{\rm pole}=0.6241$ (together with $\delta=1.7M_{\rm f}$ which is, however, less crucial) yields an excellent EOB/NR agreement. We exhibit our results in the four panels of Fig. 1.

The top-left panel of Fig. 1 compares the NR GW frequency both to the (matched) EOB GW frequency, and to twice the orbital frequency. The time axis is $t_{\rm NR}$, and/or (see above) $t_{\rm EOB}' = t_{\rm EOB} + \tau$ (with $\tau = -2032M$ for the present case). The vertical lines on the right indicate the center and the outlying "teeth" of our matching comb, which is, as explained above, centered on the maximum of the EOB or-

bital frequency (also called "EOB-light-ring"). The interval between the two vertical lines (LSO and "EOB-light-ring") defines the "plunge". The dashed vertical line on the left (at $t_{\rm NR}=1482$) indicates the crossing time of the adiabatic Last-Stable-Orbit (ω -LSO in the sense of [3]). Note that the three frequencies are initially close to each other, but that, later, 2Ω separates from $\omega_{22}^{
m NR}$ and $\omega_{22}^{
m EOB}$, which continue to be in very close agreement, except for a slight discrepancy around merger, which, within the EOB approach, is conventionally supposed to take place at the maximum of Ω . Note also the good agreement between the EOB GW frequency during the ringdown plateau, and the average of the NR one. As discussed in Sec. II the values for the mass and dimensionless spin of the final black hole that we used (together with [51]) to compute the QNMs frequencies are: $M_{\rm f}^{\rm ring} = 0.959165 M$, $j_{\rm f}^{\rm ring}=0.684639.$ The top-right panel of Fig. 1 shows the EOB-NR phase dif-

The top-right panel of Fig. 1 shows the EOB-NR phase difference, Eq. (8), ("pinched" at the two instants, $t_1^{\rm NR}$, $t_2^{\rm NR}$, given above). It is remarkable that the (two-sided) EOB-NR phase difference over the time interval (639M, 1524M) (which covers about 12 GW cycles of inspiral, plunge, and early ring-down) is smaller than about $\pm \frac{1}{2}0.068$ radians, which corresponds to ± 0.005 GW cycles.

The bottom-left panel of Fig. 1 compares the NR GW amplitude to the resummed 3^{+2} -PN accurate EOB one. It also shows the orbital frequency Ω as an help to locate the merger. One notices a very good agreement between the two amplitudes. During the interval (1100M, 1400M) the fractional EOB-NR amplitude difference varies between -1%and +1%. After $t_{NR} = 1400M$, this fractional difference increases from +1% to a maximum of +18% (reached at $t_{\rm NR} \simeq 1509 M$) and then decreases to take values of order -5% during the observationally relevant part of the ringdown. Note also that the NR equal-mass amplitude (divided by ν , i.e. by μ) time series is qualitatively, and even quantitatively, very similar to the corresponding NR test-mass amplitude time series shown in Fig. 3 of [22]. For instance, the value of the maximum amplitude is ~ 0.3 in both cases. A similar qualitative, but *not* quantitative, parallelism exists for the two corresponding frequency time series (the $\nu = 1/4$ frequency levelling off at a higher "plateau").

Finally, the bottom-right panel of Fig. 1 compares the real parts of the NR and EOB waveforms. The two vertical lines delimit the interval between LSO and "EOB-light-ring". Again the agreement between the two waveforms is impressive. Note that this last panel shows only the late inspiral, plunge and ringdown. From the panel showing the phase difference, one can gather that the agreement stays as impressive over a much longer time span of order 1000M (essentially from $t_{\rm NR} \sim 500M$ to the end of ringdown).

B. Comparing NR to resummed EOB for $a_5 = 60$

Let us now consider our second representative value of the effective 4 PN radial potential parameter, $a_5=60$. As before we chose $\delta=1.7M_{\rm f}$. We also selected the same phase "pinching" interval as above. Then, by trial and error, we

¹⁰ Though we did not investigate thoroughly what "error bar" can be put on such a "best" value of $v_{\rm pole}$, the numerical studies we did indicate that a change of ± 2 on the last (i.e. fourth) digit that we quote is sufficient to entail a visible worsening of the phase difference $\Delta \phi_{\rm 2C}^{\rm 2DBNR}$.

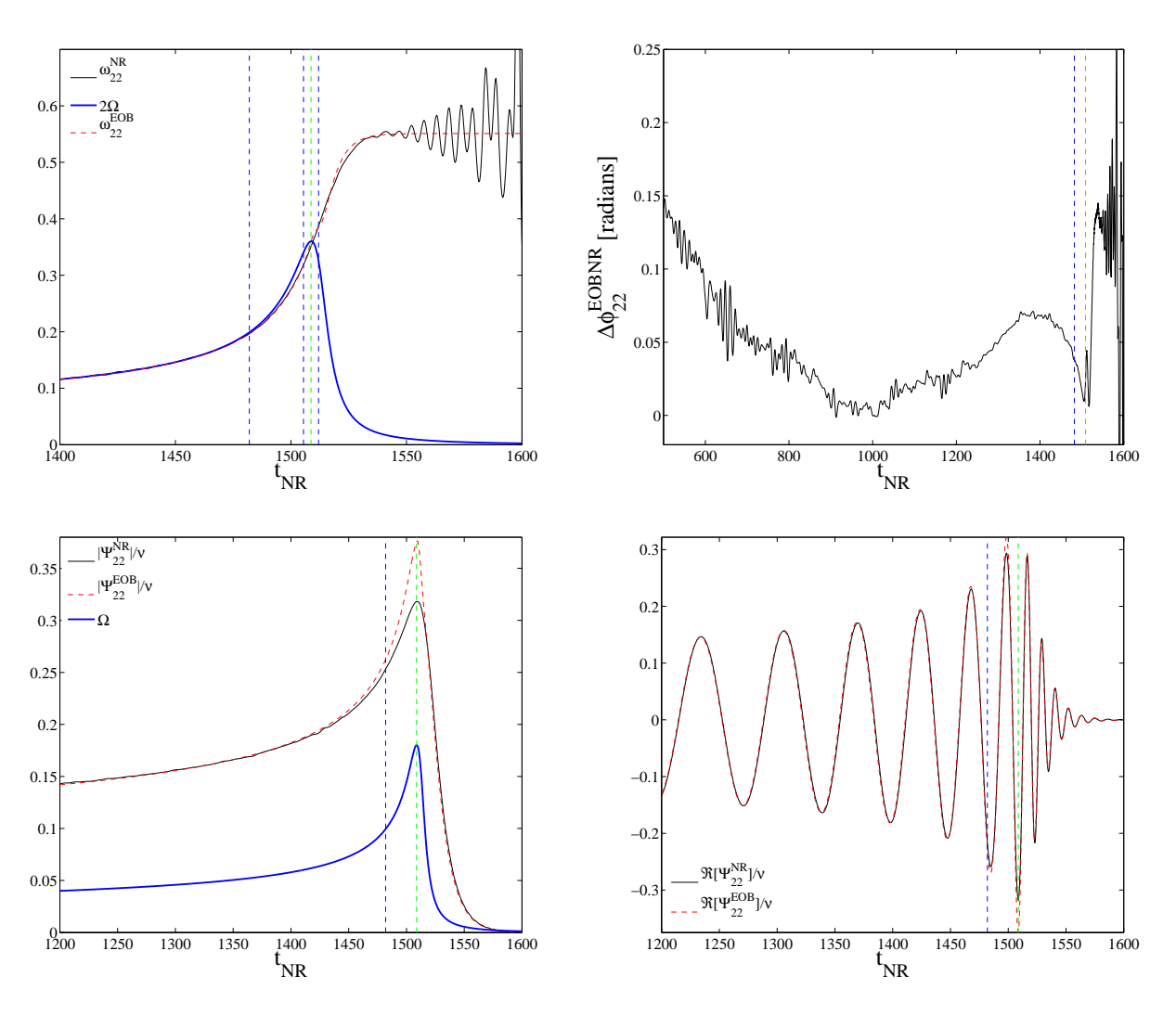


FIG. 1: Comparison between EOB and NR waveforms for $a_5=25$ and $v_{\rm pole}=0.6241$: frequencies (top-left), phase difference (top-right), amplitudes (bottom-left) and real parts (bottom-right) of the two gravitational waveforms. The vertical line at $t_{\rm NR}=1509$ locates the maximum of (twice) the orbital frequency Ω (alias the "EOB-light-ring") and indicates the center of our matching comb (whose total width is indicated by the two neighboring vertical lines in the top-left panel). The vertical dashed line at $t^{\rm NR}=1482$ indicates the crossing time of the adiabatic LSO orbital frequency ($\Omega_{\rm LSO}=0.1003$).

found that $v_{\rm pole}=0.5356$ yields an excellent EOB/NR agreement $^{11}.$

We exhibit our results in the four panels of Fig. 2, which are entirely parallel to those of Fig. 1. The remarkable level of EOB/NR agreement that we get now, when $a_5=60$, is rather close to the one that we got above when $a_5=25$. At this stage, there is no rationale for saying that either value of a_5 is preferred over the other (though $a_5=25$ yields somewhat better results). Some partial numerical tests that we performed suggest that this conclusion extends to (at least) all values of a_5 between 25 and 60.

Some of the numbers quantifying the EOB/NR agreement are:

(i) the (two-sided) EOB-NR phase difference over the time interval (500M,1550M) (which covers about 13 GW cycles of inspiral, plunge, and most of the ring-down) is smaller than about $\pm\frac{1}{2}0.13$ radians, which corresponds to ±0.01 GW cycles;

(ii) during the interval (1100M, 1400M) the fractional EOB-NR amplitude difference varies between -0.8% and +0.55%. After $t_{\rm NR}=1400M$, this fractional difference increases from +0.55% to a maximum of +23% (reached at $t_{\rm NR}\simeq 1511M$) and then decreases to take values of order +6% during the observationally relevant part of the ringdown.

 $^{^{11}}$ Note that this "best" value of $v_{\rm pole}$ (for $a_5=60$ and $\nu=1/4$) happens to be numerically close to the best fitting $v_{\rm pole}\simeq 0.53$ value that Ref. [24] found in the test-mass limit $\nu\to 0$.

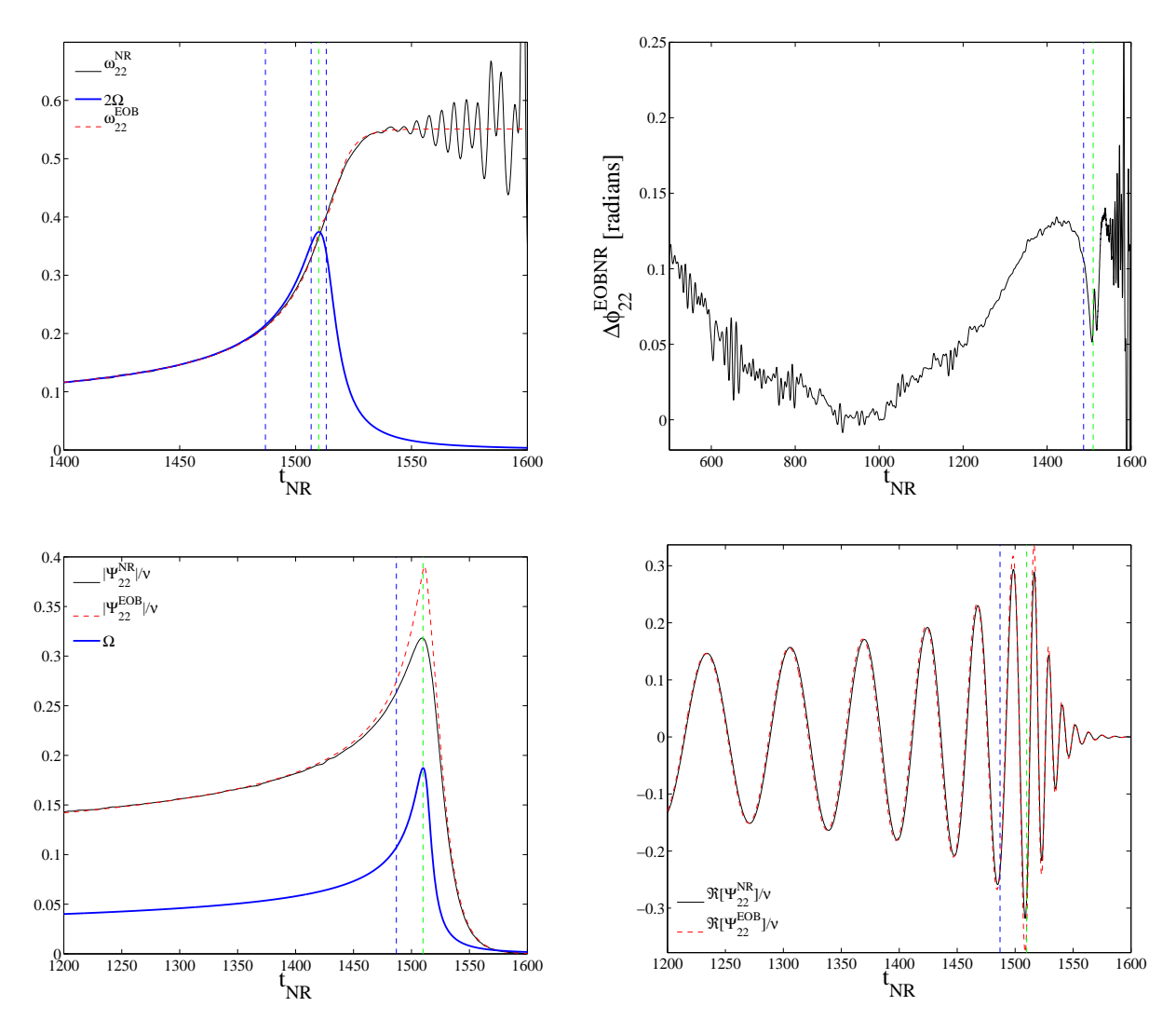


FIG. 2: Comparison between EOB and NR waveforms for $a_5=60$, $v_{\rm pole}=0.5356$: frequencies (top–left), phase difference (top–right), amplitudes (bottom–left) and real parts (bottom–right) of the two gravitational waveforms. The vertical line at $t_{\rm NR}=1510$ locates the maximum of (twice) the orbital frequency Ω (alias the "EOB-light-ring") and indicates the center of our matching comb (whose total width is indicated by the two neighboring vertical lines in the top–left panel). The vertical dashed line at $t^{\rm NR}=1487$ indicates the crossing time of the adiabatic LSO orbital frequency ($\Omega_{\rm LSO}=0.1081$).

C. Contrasting resummed EOB with restricted EOB, for $a_5=60$, by comparing NR to a standard restricted EOB waveform

Finally, we wish to illustrate the importance (for reaching a high level of faithfulness) of the various ingredients used in our present, resummed version of EOB (using a time-extended "comb matching" to 5 QNMs) by comparing NR to the type of simpler implementation of the EOB framework used in [23]. Using again $a_5=60$ (which was chosen as best value in [23]), we compare NR to the following implementation of EOB:

- we use for $v_{\rm pole}$ the "standard" value $v_{\rm pole}^{\rm DIS}(\nu)$ advocated in [1].
- we use (as originally proposed in Ref. [3]) the following

(Newtonian-order and Kepler-law-assuming) restricted quadrupole waveform

$$\Psi_{22}^{\rm NK}(t) = -4\nu \sqrt{\frac{\pi}{30}} \Omega^{2/3} \exp(-2i\Phi) , \qquad (9)$$

without any explicit PN (F_{22}) corrections, nor any NQC (a,b) corrections.

- we use only 3 (positive-frequency) QNMs.
- and, we match the plunge and ring-down waveforms in a very small interval ($\delta/M_{\rm f}=0.2$ instead of our preferred 1.7) around the maximum of the orbital frequency. [Indeed, the matching of the two waveforms and their derivatives at a sharply defined moment is

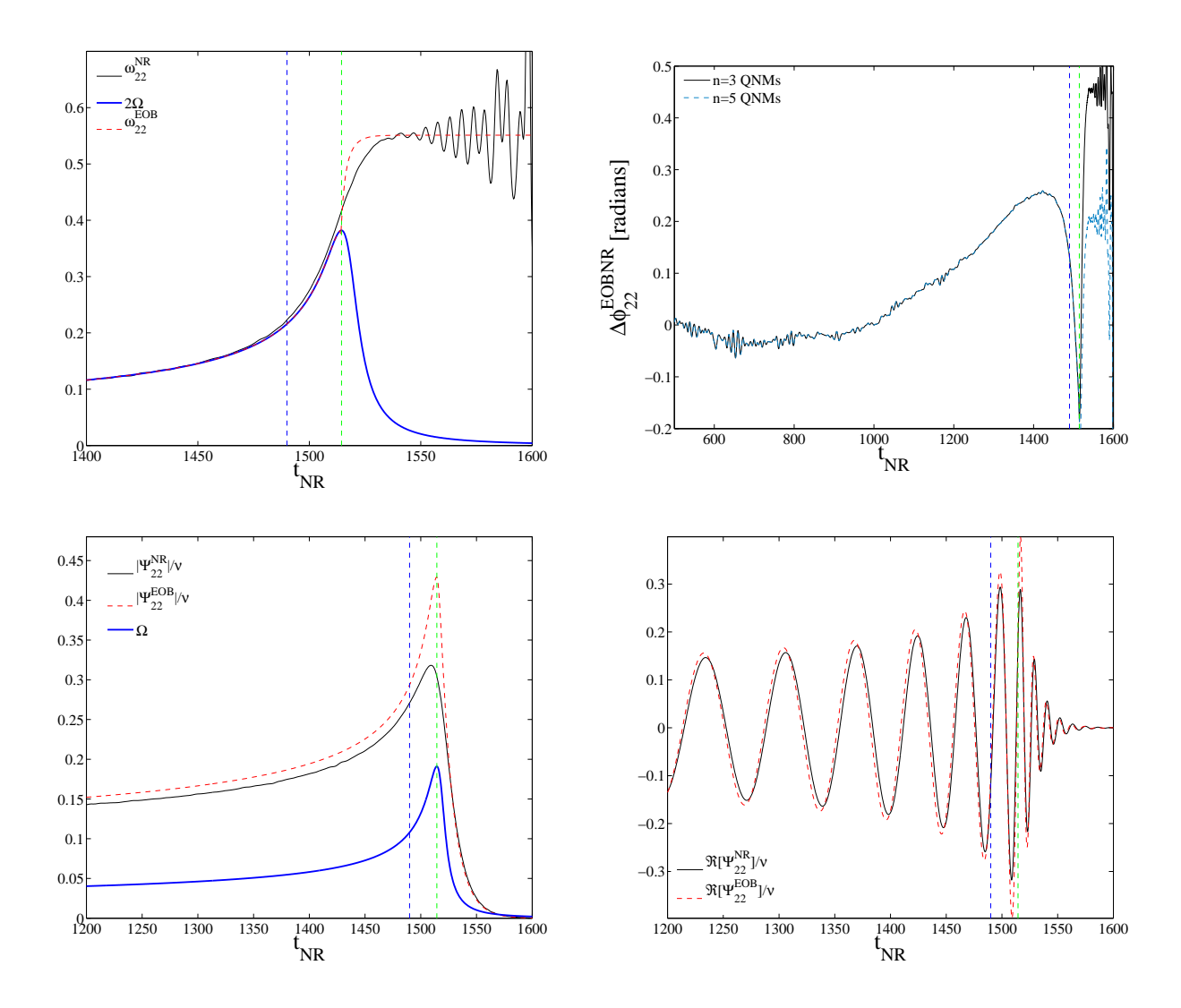


FIG. 3: Comparison between the EOB restricted waveform approximation, Eq. (9), and NR for $a_5=60$ and $v_{\rm pole}=v_{\rm pole}^{\rm DIS}(\nu=1/4)=0.6907$: frequencies (top–left), phase difference (top–right), amplitudes (bottom–left) and real parts (bottom–right) of the two gravitational waveforms. The vertical line at $t_{\rm NR}=1510$ locates the maximum of (twice) the orbital frequency Ω (alias the "EOB-light-ring") and indicates the matching time. The vertical dashed line at $t_{\rm NR}=1490$ indicates the crossing time of the adiabatic LSO orbital frequency ($\Omega_{\rm LSO}=0.1081$).

equivalent to considering the $\delta \to 0$ limit of our combmatching technique].

The results of such a coarser EOB implementation are shown in Fig. 3 (which is parallel to the previous two figures). By contrasting Fig. 3 with Fig. 2 (which used the *same value* of a_5), we see that:

 the EOB frequency agrees less well with the NR one than before, especially around the matching point. Note in particular that the post-matching analytical frequency jumps up from the maximum (doubled) orbital frequency significantly more vertically than before, thereby decoupling too soon from the exact frequency, and accruing a larger dephasing than before (because of the too localized matching, and – to a lesser degree – the use of only 3 QNMs).

- the EOB-NR (maximal) phase difference over the same time interval (500M, 1524M) is about 2.2 times larger than before. One now ends up with a phase difference of ±½0.29 radians, i.e. 0.023 GW cycles over about 13 GW cycles. The top-right panel of Fig. 3 illustrates the fact that matching with 5 QNMs (dashed line) reduces the dephasing accumulated during the transition from merger to ringdown.
- the modulus of the analytical waveform is now distinctly larger than the NR one during the inspiral (because of the lack of PN corrections).

- the modulus also exhibits a more significant discrepancy (+35%) with the NR one at the end of the plunge (because of the use of the Kepler-law-assuming $\propto \Omega^{2/3}$, which, as pointed out in [53], tends to overestimate the amplitude).
- Note also that one visually notices these differences at the level of the GW waveforms.
- The same resummed-EOB/restricted-EOB comparison was done in [22], in the $\nu\ll 1$ case, with similar conclusions.

In spite of these relative blemishes, note, however that this "coarser" EOB-type implementation still succeeds in following the phase of the exact signal to ± 0.023 GW cycles over about 13 GW cycles.

Note that the corresponding EOB/NR agreement exhibited in Fig. 4 of Ref. [23] seems to be somewhat better¹² than the one exhibited by our Fig. 3. This difference might have several origins, notably: (i) a difference in the accuracy of the NR data¹³, and (ii) a difference in the procedure used to best shift time and phase between EOB and NR data.

V. CONCLUSIONS

We have compared a recently proposed, resummed 3^{+2} -PN accurate Effective-One-Body (EOB) waveform to the result of a numerical simulation of a coalescing equal-mass binary black hole performed at the Albert Einstein Institute. We find a remarkable agreement, both in phase and in amplitude, between the new EOB waveform and the numerical data. More precisely, we find that the maximal dephasing between EOB and numerical relativity (NR) can be reduced below ± 0.005 GW cycles over the last $\sim 900M$ (corresponding to about 12 GW cycles plus ringdown ones) of the simulation. This level of agreement was exhibited for two representative values of the effective 4 PN parameter a_5 , namely $a_5 = 25$ and $a_5 = 60$, and for a corresponding, appropriately "flexed" value of the radiation-reaction resummation parameter v_{pole} . In addition, our resummed EOB amplitude agrees to better than the 1% level with the NR one up to the late inspiral.

We have also compared the NR data to a coarser implementation of the EOB approach (restricted waveform, standard $v_{\rm pole}^{\rm DIS}$, instantaneous matching to 3 QNMs). The EOB/NR agreement is slightly less good in this case, though the phase agreement remains quite good (± 0.023 GW cycles over the last $\sim 1000M$ of the simulation).

Let us point out a notable feature of our results. In the recent work of Damour and Nagar [24], the same resummed 3⁺²-PN accurate EOB waveform was compared to a long, very accurate equal-mass inspiral simulation of the Caltech-Cornell group [18]. It was found that an excellent EOB/NR agreement was obtained when a_5 and $v_{\rm pole}$ were following the rather precise correlation plotted in the upper panel of Fig. 3 of Ref. [24]. Let us denote this correlation as $a_5 \to v_{\rm pole}^{\rm best \, inspiral}(a_5)$. In the present paper, we similarly found that the EOB/NR agreement was at its best when, for a given a_5 , 14 v_{pole} was taking a rather precise corresponding "best fit value", say $v_{\text{pole}}^{\text{best insplunge}}(a_5)$. In particular, we found $v_{\rm pole}^{\rm best\,insplunge}(25)=0.6241$ and $v_{\text{pole}}^{\text{best insplunge}}(60) = 0.5356.$ On the other hand, the results of [24] yield $v_{\rm pole}^{\rm best\,inspiral}(25)=0.5340,$ and $v_{\mathrm{pole}}^{\mathrm{best\,inspiral}}(60) = 0.4856.$ The differences between these set of values are $v_{\rm pole}^{\rm best\,insplunge}(25)-v_{\rm pole}^{\rm best\,inspiral}(25)=0.0901$ and $v_{\rm pole}^{\rm best\,insplunge}(60)-v_{\rm pole}^{\rm best\,inspiral}(60)=0.0500$. Note also that the "best insplunge" $v_{\rm pole}$ values are in between the "best inspiral" ones and the originally advocated [1] one $v_{\mathrm{pole}}^{\mathrm{DIS}}(\nu=1/4)=0.6907.$ This finding will deserve further investigation in the future. At this stage we can only speculate on the various possible origins of this difference: (i) it might be due to the fact that, not having access to the original NR data of [18], Damour and Nagar had to rely on rather coarse measurements extracted from published figures; (ii) it might be due to systematic errors in the NR data of [18]; (iii) it might alternatively come from systematic errors in the NR data used in the present paper; (iv) it might come from the fact that the "best-fit" $\mathcal{F}_{\varphi}(v_{\mathrm{pole}})$ is not a uniform approximation (as a function of frequency) to the exact radiation reaction (see, in the $\nu \to 0$ limit, the bottom panels of Fig. 1 in [24]) and, finally, (v) it might come from some "missing physics" in the resummed EOB waveform explored here. There are several candidates for this missing physics. One suggestion (which follows the original suggestion of [5]) is that one might need to consider still higher (uncalculated) PN contributions to the radial EOB potential¹⁵ $A(u) = 1 - 2u + 2\nu u^3 + a_4\nu u^4 + a_5\nu u^5 + a_6\nu u^6 + \cdots$ where u = 1/r. Another suggestion is that non-quasi-circular (NOC) corrections to radiation reaction might modify the phasing during late inspiral and plunge. As an example, we have looked at this possibility. More precisely, following [22], we can introduce a new flexibility parameter $\bar{a}^{\mathrm{RR}\ 16}$ such that the radiation reaction force is multiplied by a correction factor $f_{\rm RR}^{
m NQC}$ given by

 $^{^{12}}$ The reader should however keep in mind that in Fig. 4 of Ref. [23] the EOB-NR phase difference is divided by 2π compared to the one showed in our Fig. 3.

¹³ The data used in [23] were not benefitting from the reduction in eccentricity used in the data considered here.

 $^{^{14}}$ Though we did not explore all possible values of a_5 , we sampled intermediate values between the representative a_5 values we picked and convinced ourselves that the same conclusion held for them.

 $^{^{15}}$ For simplicity, we consider only linear-in- ν higher PN contributions. If the need arises (and the fact that the unequal-mass EOB/NR comparisons of [23] seem to exhibit a strong dependence on the mass ratio might suggest it) one can easily add in a non-linear ν dependence.

Actually [22] introduced a parameter $a^{\rm RR}$ which is, roughly, the negative of $\bar{a}^{\rm RR}$, with a NQC radiation reaction factor of the form $1+a^{\rm RR}p_{r_*}^2/(r\Omega)^2$

$$f_{\rm RR}^{\rm NQC} = \left(1 + \bar{a}^{\rm RR} \frac{p_{r_*}^2}{(r\Omega)^2 + \epsilon}\right)^{-1}$$
 (10)

Such a factor will be very close to one during the inspiral (and therefore be negligible in the EOB comparison to the Caltech-Cornell data), but will start being significantly less than one (if $\bar{a}^{RR} > 0$) during the late inspiral and plunge, which are of interest for the comparison to the presently considered data. And indeed, we have found that by choosing a value $\bar{a}^{\rm RR} \sim +40$ (and $\epsilon = 0.12$ as in the waveform NQC factor considered above) we could, when $a_5 = 25$, obtain an excellent EOB/NR fit by using the "best inspiral" value $v_{
m pole}^{
m best \, inspiral}(25) = 0.5340$ (instead of the above $v_{
m pole}^{
m best \, insplunge}(25) = 0.6241).$ However, this result is not quite satisfactory because the numerical value $\bar{a}^{RR} \sim +40$ is uncomfortably higher than the a priori expected $\bar{a}^{RR} \sim {\cal O}(1)$. Anyway, as said above, this issue needs to be further investigated by using the most accurate possible data covering both inspiral and plunge. We hope to come back to it in the future.

Finally, we think that the present work, taken in conjunc-

tion with other recent works on the EOB/NR comparison, confirms the ability of the EOB formalism to accurately capture the general-relativistic waveforms. The present work has also shown that the recently proposed resummed 3⁺²-PN accurate waveform is important for defining analytical EOB waveforms wich faithfully represent (both in phase and in amplitude) the waveforms emitted by equal-mass coalescing (nonspinning) black hole binaries.

Acknowledgments

We thank Peter Diener for assistance and discussion in the early stages of this work, Sascha Husa for help with the NR initial data, and Sebastiano Bernuzzi for help in the analysis of the ringdown waveform. The NR computations were performed with the Damiana, Belladonna and Peyote clusters of the Albert Einstein Institute. This work was supported in part by DFG grant SFB/Transregio 7 "Gravitational Wave Astronomy". The commercial software products Mathematica TM and Matlab have been extensively used in the preparation of this paper.

- [1] T. Damour, B. R. Iyer and B. S. Sathyaprakash, Phys. Rev. D 57, 885 (1998) [arXiv:gr-qc/9708034].
- [2] A. Buonanno and T. Damour, Phys. Rev. D 59, 084006 (1999) [arXiv:gr-qc/9811091].
- [3] A. Buonanno and T. Damour, Phys. Rev. D 62, 064015 (2000) [arXiv:gr-qc/0001013].
- [4] T. Damour, P. Jaranowski and G. Schaefer, Phys. Rev. D 62, 084011 (2000) [arXiv:gr-qc/0005034].
- [5] T. Damour, Phys. Rev. D 64, 124013 (2001) [arXiv:gr-qc/0103018].
- [6] A. Buonanno, Y. Chen and T. Damour, Phys. Rev. D 74, 104005 (2006) [arXiv:gr-qc/0508067].
- [7] F. Pretorius, Phys. Rev. Lett. 95, 121101 (2005) [arXiv:gr-qc/0507014].
- [8] M. Campanelli, C. O. Lousto, P. Marronetti and Y. Zlochower, Phys. Rev. Lett. 96, 111101 (2006) [arXiv:gr-qc/0511048].
- [9] M. Campanelli, C. O. Lousto and Y. Zlochower, Phys. Rev. D 74, 041501(R) (2006) [arXiv:gr-qc/0604012].
- [10] J. G. Baker, J. Centrella, D. I. Choi, M. Koppitz and J. van Meter, Phys. Rev. D 73, 104002 (2006) [arXiv:gr-qc/0602026].
- [11] J. G. Baker, J. Centrella, D. I. Choi, M. Koppitz, J. R. van Meter and M. C. Miller, Astrophys. J. 653, L93 (2006) [arXiv:astroph/0603204].
- [12] J. G. Baker, M. Campanelli, F. Pretorius and Y. Zlochower, Class. Quant. Grav. 24, S25 (2007) [arXiv:gr-qc/0701016].
- [13] J. A. Gonzalez, U. Sperhake, B. Brügmann, M. Hannam and S. Husa, Phys. Rev. Lett. 98, 091101 (2007) [arXiv:gr-qc/0610154].
- [14] S. Husa, J. A. Gonzalez, M. Hannam, B. Brugmann and U. Sperhake, arXiv:0706.0740 [gr-qc].
- [15] M. Koppitz, D. Pollney, C. Reisswig, L. Rezzolla, J. Thornburg, P. Diener and E. Schnetter, Phys. Rev. Lett. 99,041102 (2007) [arXiv:gr-qc/0701163].
- [16] L. Rezzolla, E. N. Dorband, C. Reisswig, P. Diener, D. Pollney, E. Schnetter and B. Szilagyi, arXiv:0708.3999 [gr-qc].

- [17] L. Rezzolla, P. Diener, E. N. Dorband, D. Pollney, C. Reisswig, E. Schnetter and J. Seiler, Astrophys. J. *in press* arXiv:0710.3345 [gr-qc].
- [18] M. Boyle, D.A. Brown, L.E. Kidder, A.H. Mroué, H.P. Pfeiffer, M.A. Scheel, G.B. Cook and S.A. Teukolsky arXiv:0710.0158 [gr-qc].
- [19] A. Buonanno, G. B. Cook and F. Pretorius, Phys. Rev. D 75, 124018 (2007) [arXiv:gr-qc/0610122].
- [20] Y. Pan et al., arXiv:0704.1964 [gr-qc].
- [21] T. Damour and A. Nagar, Phys. Rev. D 76, 044003 (2007).
- [22] T. Damour and A. Nagar, Phys. Rev. D **76**, 064028 (2007) [arXiv:0705.2519 [gr-qc]].
- [23] A. Buonanno, Y. Pan, J. G. Baker, J. Centrella, B. J. Kelly,S. T. McWilliams and J. R. van Meter, Phys. Rev. D 76, 104049 (2007) [arXiv:0706.3732 [gr-qc]].
- [24] T. Damour and A. Nagar, arXiv:0711.2628 [gr-qc].
- [25] A. Nagar, T. Damour and A. Tartaglia, Class. Quant. Grav. 24, S109 (2007) [arXiv:gr-qc/0612096].
- [26] T. Damour, B. R. Iyer, P. Jaranowski and B. S. Sathyaprakash, Phys. Rev. D 67, 064028 (2003) [arXiv:gr-qc/0211041].
- [27] T. Damour, E. Gourgoulhon and P. Grandclement, Phys. Rev. D **66**, 024007 (2002) [arXiv:gr-qc/0204011].
- [28] P. Ajith, et al. Class. Quantum Grav. 24 S689 (2007) [arXiv:0704.3764]
- [29] P. Ajith, et al. Phys. Rev. D in press (2007) [arXiv:0710.2335]
- [30] D. Pollney *et al.*, Phys. Rev. D **76**, 124002 (2007) [arXiv:0707.2559 [gr-qc]].
- [31] T. Goodale, G. Allen, G. Lanfermann, J. Massó, T. Radke, E. Seidel, and J. Shalf, in *Vector and Parallel Processing*, VECPAR'2002, 5th International Conference, Lecture Notes in Computer Science Springer, Berlin, (2003)
- [32] C. Bona, J. Masso, E. Seidel and J. Stela, Phys. Rev. Lett. **75**, 600 (1995) [arXiv:gr-qc/9412071].
- [33] M. Alcubierre, B. Brugmann, P. Diener, M. Koppitz, D. Pollney, E. Seidel and R. Takahashi, Phys. Rev. D 67, 084023 (2003)

- [arXiv:gr-qc/0206072].
- [34] J. G. Baker, J. Centrella, D. I. Choi, M. Koppitz and J. van Meter, Phys. Rev. Lett. 96, 111102 (2006) [arXiv:gr-qc/0511103].
- [35] E. Schnetter, S. H. Hawley, and I. Hawke, Class. Quantum Grav. 21, 1465 (2004)
- [36] J. Thornburg, Class. Quantum Grav. 21, 743 (2004)
- [37] A. Nagar and L. Rezzolla, Class. Quant. Grav. 22, R167 (2005) [Erratum-ibid. 23, 4297 (2006)] [arXiv:gr-qc/0502064].
- [38] D. R. Brill and R. W. Lindquist, Phys. Rev. 131, 471 (1963).
- [39] S. Brandt and B. Brugmann, Phys. Rev. Lett. **78**, 3606 (1997) [arXiv:gr-qc/9703066].
- [40] M. Ansorg, B. Brugmann and W. Tichy, Phys. Rev. D 70, 064011 (2004) [arXiv:gr-qc/0404056].
- [41] G. B. Cook, Phys. Rev. D 50, 5025 (1994) [arXiv:gr-qc/9404043].
- [42] H. P. Pfeiffer, D. A. Brown, L. E. Kidder, L. Lindblom, G. Lovelace and M. A. Scheel, Class. Quant. Grav. 24, S59 (2007) [arXiv:gr-qc/0702106].
- [43] S. Husa, M. Hannam, J. A. Gonzalez, U. Sperhake and B. Brugmann, arXiv:0706.0904 [gr-qc].
- [44] T. Damour, P. Jaranowski and G. Schafer, Phys. Lett. B 513, 147 (2001) [arXiv:gr-qc/0105038].
- [45] L. Blanchet, T. Damour, G. Esposito-Farese and B. R. Iyer,

- Phys. Rev. Lett. 93, 091101 (2004) [arXiv:gr-qc/0406012].
- [46] O. Dreyer, B. Krishnan, D. Shoemaker and E. Schnetter, Phys. Rev. D 67, 024018 (2003) [arXiv:gr-qc/0206008].
- [47] A. Ashtekar and B. Krishnan, Phys. Rev. D 68, 104030 (2003) [arXiv:gr-qc/0308033].
- [48] E. N. Dorband, E. Berti, P. Diener, E. Schnetter and M. Tiglio, Phys. Rev. D 74, 084028 (2006) [arXiv:gr-qc/0608091].
- [49] E. Berti, V. Cardoso, J. A. Gonzalez and U. Sperhake, Phys. Rev. D 75, 124017 (2007) [arXiv:gr-qc/0701086].
- [50] E. Berti, V. Cardoso, J. A. Gonzalez, U. Sperhake, M. Hannam, S. Husa and B. Bruegmann, Phys. Rev. D 76, 064034 (2007) [arXiv:gr-qc/0703053].
- [51] E. Berti, V. Cardoso and C. M. Will, Phys. Rev. D 73, 064030 (2006) [arXiv:gr-qc/0512160].
- [52] M. Davis, R. Ruffini and J. Tiomno, Phys. Rev. D 5, 2932 (1972).
- [53] T. Damour and A. Gopakumar, Phys. Rev. D 73, 124006 (2006) [arXiv:gr-qc/0602117].
- [54] W. H. Press and S. A. Teukolsky, Astrophys. J. 185, 649 (1973).
- [55] H. Onozawa, Phys. Rev. D 55, 3593 (1997) [arXiv:gr-qc/9610048].